

# Landé g-tensor in semiconductor nanostructures

T. P. Mayer Alegre,<sup>1,2</sup> F. G. G. Hernández,<sup>1,2</sup> A. Pereira,<sup>1</sup> and G. Medeiros-Ribeiro<sup>1</sup>

<sup>1</sup>*Laboratório Nacional de Luz Síncrotron, Campinas, SP, Brazil*

<sup>2</sup>*Instituto de Física Gleb Wataghin Universidade Estadual de Campinas, Campinas, SP, Brazil*

Understanding the electronic structure of semiconductor nanostructures is not complete without a detailed description of their corresponding spin-related properties. Here we explore the response of the shell structure of InAs self-assembled quantum dots to magnetic fields oriented in several directions, allowing the mapping of the g-tensor modulus for the s and p-shells. We found that the g-tensors for the s and p shells show a very different behavior. The s-state in being more localized allows the probing of the confining potential details by sweeping the magnetic field orientation from the growth direction towards the in-plane direction. As for the p-state, we found that the g-tensor modulus is closer to that of the surrounding GaAs, consistent with a larger delocalization. These results reveal further details of the confining potentials of self-assembled quantum dots that have not yet been probed, in addition to the assessment of the g-tensor, which is of fundamental importance for the implementation of spin related applications.

Electronic magnetism in semiconductor nanostructures is one of the important properties to be harnessed in spintronic devices [1] as well as in prototypical systems for quantum information processing[2]. In order to understand and separate the effects of quantum confinement and band structure, including spin-orbit coupling, strain and non-parabolic effects, the response of the electronic spin on an applied static magnetic field can provide an improved picture of the overall quantum system. The electronic g tensor, which describes the symmetries and magnetic response of the unpaired electron system, is thus a very important tool to assess and investigate these fundamental aspects of spin electronics in nanostructures.

For conduction electrons in bulk semiconductor crystals, the g-factor can be determined accurately by second order  $\mathbf{k} \cdot \mathbf{p}$  theory by the so-called Roth's equation[3, 4], and confirmed by experiment [5]. For unpaired electrons bound to donors, g-tensor differences from the free atom value of 2 for the ground state will reveal the dependence on the crystal field and spin-orbit coupling[6]. In addition to that, the anisotropic part of  $g$  is a determining factor for spin-lattice relaxation and thus of great importance for any spin related applications [7, 8]. For the case of quantum wells[9] and wires [10] the g-tensor will be affected by quantum confinement, strain and composition fluctuations.

For the case of quantum dots (QDs), whereas one is interested in metallic nanoparticles [11] or lithographically defined QDs [12, 13], there has been a number of reports covering the topic. For metallic nanoparticles, the difficulties arise in finding the symmetry axis, which can be determined from the g-tensor mapping. Nevertheless is important to mention that for this case, the electron mean free path is smaller than the size of the particle, and hence the angular momentum may not be a good quantum number. For the case of 2DEG lithographically defined quantum dots, the Zeeman splitting and the orbital splitting have comparable energy scales,

thus preventing the evaluation of the g-factor for an out-of-plane magnetic field configuration. However for self-assembled quantum dots, a number of experiments have demonstrated striking similarities with the atomic behavior, like Hund rules and Aufbau principle in determining the shell filling for electrons [14, 15]. The charging, Zeeman splitting and single particle energies are very different for this case, which allows one the investigation of each effect, for excitons and electrons [16, 17, 18, 19]. More recently, calculations were carried out displaying the relationship between the g-tensor and the electronic structure for quantum dots[20].

In this Letter we explore the shell structure dependent spin properties of electrons trapped in InAs quantum dots (QDs). By evaluating the electron addition energies inferred from magneto-capacitance data, we present an experimental account on the g-tensor modulus for the s and p states which were mapped out according to the crystallographic directions of highest symmetry.

InAs QDs were grown by molecular beam epitaxy and capped with thin InGaAs strain reducing layers, as described in previous publications[18, 19]. These structures were embedded in capacitance structures that were subsequently defined by conventional photolithography. The area of the devices was  $4 \times 10^{-2} \text{mm}^2$ , hence encompassing an ensemble of about  $10^8$  QDs per device. Magnetocapacitance experiments were carried out at 2.7K for magnetic field intensities ranging from 0 to 15T. Field sweeps were performed at  $15^\circ$  intervals covering at least  $180^\circ$  by tilting the sample with a goniometer.

Figure 1 (a) shows the second derivative of magneto-capacitance spectra taken for field sweeps along the [001] and [110] directions (polar scan). The energy scale derived from the applied bias and voltage-dependent lever arm is translated into the chemical potential within the QDs referenced to the GaAs conduction band-edge. The lever arm was calculated taken into account depletion effects in the back contact[19], thus allowing the determination of a precise energy scale. The gray scale map is a repre-

sensation of the density of states (DOS), where the 0D (up to  $\sim -80\text{meV}$ ) and 2D (above  $\sim -80\text{meV}$ ) levels associated to the QDs and wetting layer can be easily identified. It is interesting to note that for in-plane field all orbital effects are minimized given the pancake geometry of the quantum dots; also negligible are the effects of the magnetic field on the wetting layer, which exhibits Landau level fillings for magnetic fields perpendicular to the sample surface.

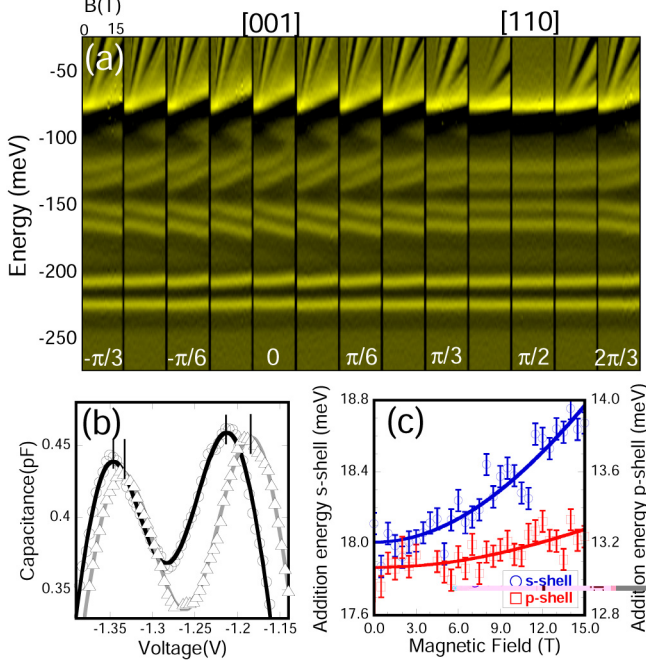


FIG. 1: **(a)** Measured data (derivative) for polar scan, *i.e.*, magnetic field sweeping from parallel to  $[001]$  direction towards  $[110]$  direction. **(b)** Different capacitance spectra showing the filling of the s-shell with 1 and 2 electrons, dots correspond to  $\mathbf{B} = 0\text{T}$  and triangle to  $|\mathbf{B}| = 15\text{T}$ , and  $\theta = \pi/12$ . The solid lines correspond to two gaussian fits. **(c)** Fits to equation 1 for s and p-shell electron addition energies for  $\theta = \pi/2$ .

From the electron addition energies [15, 18, 19], orbital, electrostatic and Zeeman contributions were separated. Figure 1 (b) shows the shift of the capacitance peaks for the sequential charging of the s-level on the applied magnetic field for  $\theta = \pi/12$ . The effects of Coulomb charging, diamagnetic shifts and Zeeman splitting can be seen in these data. One can separate the orbital effect contribution from the others by subtracting the peak positions, as the diamagnetic contribution is the same for both. For the s-shell, using a Fock-Darwin (FD) formalism[14, 19] one has for the loading of the first and second electron for  $T=0$  and  $\mathbf{B} \parallel [001]$ :  $E_{s1} = E_z + \hbar\Omega - |g_{zz}|\beta\mathbf{B}/2$ ;  $E_{s2} = E_{s1} + |g_{zz}|\beta\mathbf{B} + E_C^s$ , where  $E_z$  is the confinement along the growth direction,  $\Omega = \sqrt{\omega_0^2 + \omega_c^2}/4$ , with  $\omega_c$  as the cyclotron frequency,  $E_C^s$  the Coulomb charging energy at zero magnetic field

for the s-shell electrons, and  $|g_{zz}|\beta\mathbf{B}$  the Zeeman splitting. For the s-shell, one finds  $\hbar\omega_0 = 37.8 \pm 0.2\text{meV}$  and  $E_z \sim -280\text{meV}$ . More detailed modeling can provide an even better description [15], however it is not necessary to capture the features that we focus our efforts on. Electrostatic effects can be calculated given the single particle energies within the FD framework[14]. For the s and p shells we find  $E_{ss}=17.2\text{meV}$  and  $E_{pp}=13.4\text{meV}$ . Figure 1 (c) shows the dependence of the addition energies for the s-s and p-p configurations on the applied magnetic field for  $\theta = \pi/2$ . We find that an agreement between 5%-15% can be found from the calculated and measured addition spectra. Two effects must be considered when analyzing these data - i) wavefunction compression and its effect on the charging energies and ii) temperature.

As the magnetic field is raised, the wavefunction is compressed which increases the Coulomb charging energies. Under the FD formalism, this effect can be calculated as  $E_C^i(B) = E_C^i(0) (1 + \Omega^2/\omega_0^2)^{1/4}$ , where  $E_C^i(0)$  is the Coulomb charging energy at zero magnetic field for the *i*-shell. This effect takes place for all directions of the applied magnetic field, but to a lesser extent for the in-plane configuration due to a stronger confinement along the growth direction. As a first order approximation, we assume this effect to be the same for all configurations. The consequence of this assumption is to underestimate the Zeeman contribution for in-plane magnetic fields.

As stated above, the experiments were carried out in QDs ensembles. Thus, an accurate description of this system at finite temperatures requires the usage of a magnetization model for a system of  $n$  non-interacting spins, which can be carried out by calculating the partition function for the system. For the current analysis, we take into account the temperature dependent spin contribution on the addition energy spectra. This yields a direct relationship between the addition energy  $\Delta\mu$ , the B dependent Coulomb charging, the Zeeman splitting and the temperature:

$$\Delta\mu_s = E_{CB}(B) + 2k_B T \ln \left[ 2 \cosh \left( \frac{g\mu_B |\mathbf{B}|}{2k_B T} \right) \right] \quad (1)$$

Figure 1 (c) shows  $\Delta\mu$  as a function of the magnetic field and the corresponding fit to equation 1 for the s-shell at  $\theta = \pi/2$  (*i.e.*, in-plane magnetic field). For the p-shell, the same description applies, and a similar relation can be derived. However, the observed addition energies and the dependence on  $\mathbf{B}$  are smaller (fig. 1c), and it becomes difficult to implement a reliable fit for two additional factors: i) a smaller Coulomb charging energy  $E_C^p = 3/4 E_C^s$ , and ii) broadening of the capacitance peaks due to the Coulomb disorder which goes with  $n^2$ ,  $n$  being the number of electrons trapped inside the QDs [21]. In order to fit the data we choose  $E_C^p(B) = E_C^p(0)$  and retained the temperature dependence. Although an approximation, it is instructive to present this analysis as it represents an

upper bound on the g-tensor, and most importantly, it can help elucidating the symmetries for this particular state.

A good agreement is found for both states, and the temperature as determined from the fit to equation 1 agrees with the experimental value to within 10%. This reasonably simple description takes into account the most important factors in determining the Zeeman splitting in quantum dots, including temperature effects and wavefunction compression.

From the g factor obtained at each angle for each shell, the g tensor was determined for the polar and azimuthal scans by  $g_{pol} = \sqrt{g_{[001]}^2 \cos(\theta)^2 + g_{[110]}^2 \sin(\theta)^2}$  and  $g_{az} = \sqrt{g_{[110]}^2 \cos(\phi)^2 + g_{[1\bar{1}0]}^2 \sin(\phi)^2}$ . Figures 2 and 3 show the polar and azimuthal scans. On the top panel the experimental set-up is represented showing the orientation of the magnetic field with respect to the QD crystalline axis, as well as the FD wavefunctions for each shell calculated for  $\mathbf{B} = 15\text{T}$ . The data are shown on the bottom panel with the corresponding fits.

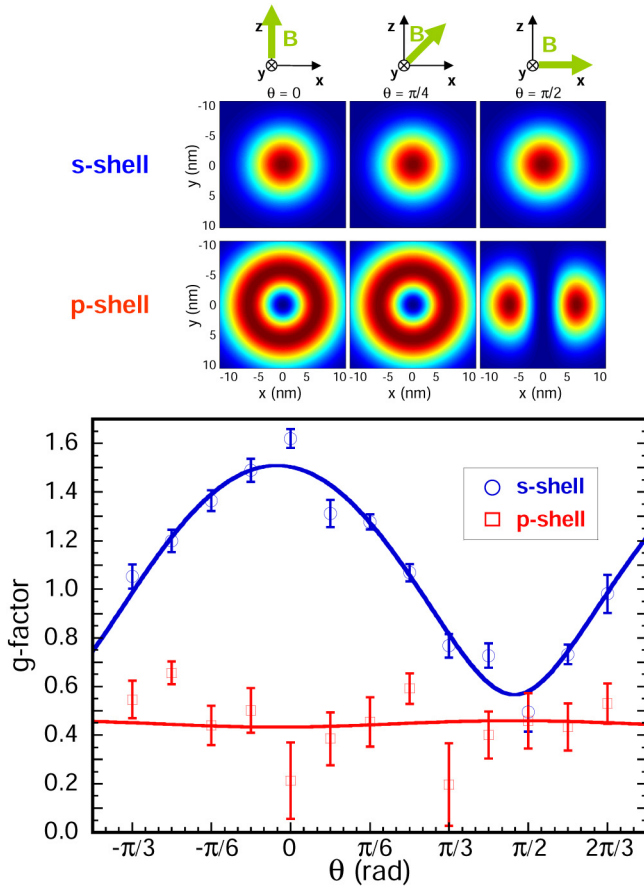


FIG. 2: (top) Wavefunction for the s and p-shell for three directions on applied magnetic field  $\theta = 0$ ,  $\theta = \pi/4$  and  $\theta = \pi/2$ .  $x, y$  and  $z$  correspond to  $[110]$ ,  $[1\bar{1}0]$  and  $[001]$  directions. (bottom) g-tensor for the s and p-shells for the polar scan.

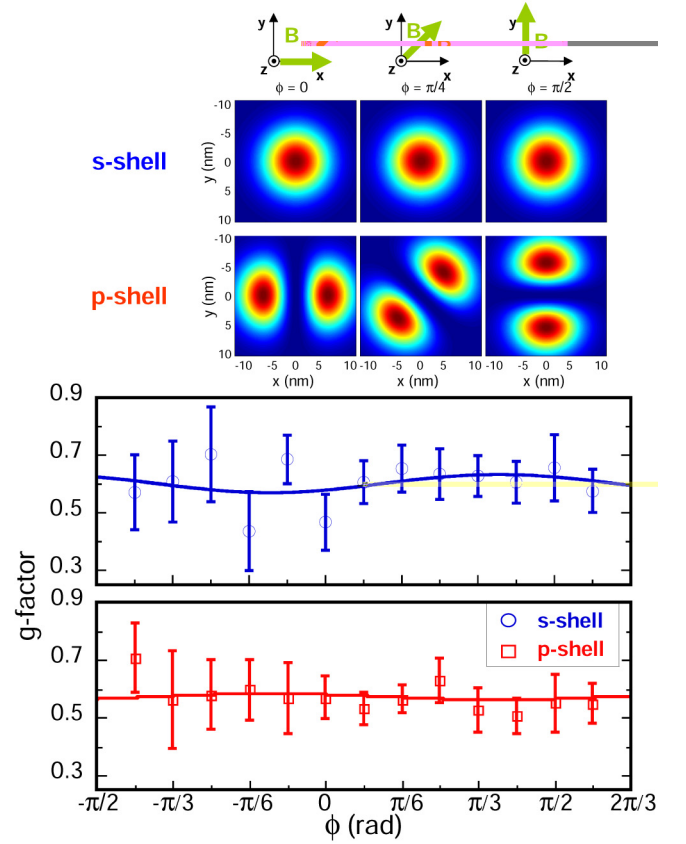


FIG. 3: (top) Wavefunction for the s and p-shell for three directions on applied magnetic field  $\phi = 0$ ,  $\phi = \pi/4$  and  $\phi = \pi/2$ .  $x, y$  and  $z$  correspond to  $[110]$ ,  $[1\bar{1}0]$  and  $[001]$  directions. (bottom) g-tensor for the s and p-shells for the azimuthal scan.

As a general observation, from the polar scan one can immediately note the effect of the strong confinement along  $z$ , being more pronounced for the s-shell and negligible for the p-shell. This is a quite surprising result at first, considering the wavefunction symmetries, the single particle energy ( $\hbar\omega_0 = 37.8\text{meV}$ ) and confinement along  $z$  ( $E_z = -280\text{meV}$ ). From the fit, we find  $g_{[001]}^s = 1.51 \pm 0.03$  and  $g_{[110]}^s = 0.57 \pm 0.05$ , and  $g_{[001]}^p \approx g_{[110]}^p = 0.47 \pm 0.07$ . Insofar as the behavior for  $g^s$  is concerned, one notes that the wavefunction is more localized into the QD and consequently more sensitive to the confinement potential details. It is expected a high anisotropy given the pancake geometry of the QDs. For the p-shell, the vertical and lateral confinement each have an effect in rendering the isotropic behavior. First, as the electrons on the p-shell are more delocalized, a leakage of the wavefunction along the growth direction takes place. Second, the wavefunction for the p-shell has a node at the center of the QDs, which permits the probing of the regions outside or at the interfaces of the QDs. Hence the g-factor tends to take the character of the surrounding matrix.

As mentioned previously,  $g_{[110]}^s$  and  $g^p$  correspond to lower and upper bounds. Yet, they are very close to the value  $|g_{GaAs}|$  of 0.44. Figure 3 shows the g-tensor for an in-plane field configuration (azimuthal scan). For both s and p shells not only the g-factor is independent of the field direction, but it is also close in modulus to the value for bulk GaAs. It is also interesting to compare these in-plane results with lithographically defined QDs, where the g-factor is about the same however it displays a dependence on the magnetic field[13], not observed in our case.

Several aspects have to be taken into account when interpreting the obtained results: i) the effect of strain which changes the details of the confining potential, ii) non-parabolic effects which take place in InAs, iii) quantum confinement effects, and iv) non-uniform composition. All these parameters may change the spin-orbit coupling, which is one of the important components in the g-factor determination. Another one is the local crystal field, which is strain dependent. The balance between all these factors will ultimately define what g factor one has. It is important to mention that it has been demonstrated that by tuning the strain in the QDs one can tailor the g-factor [19, 22], as well as by composition [23]. Finally, if one compares these experimental results with theory, a good agreement is found which corroborates the description by Pryor *et al* [20].

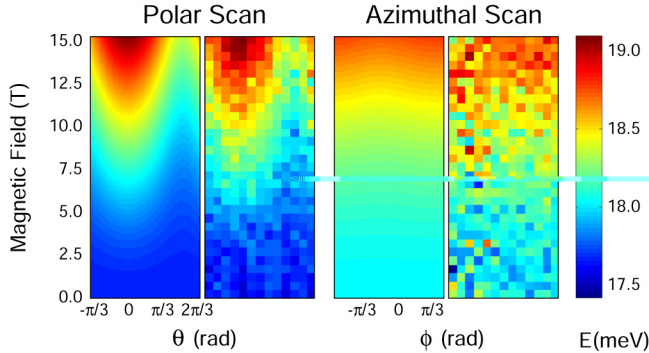


FIG. 4: (left) calculated and measured addition energies for the polar scan;(right) same for the azimuthal scan.

As a final verification of the models utilized in this work, we calculate the electron addition energy for  $n=2$ , *i.e.*, s-shell filling, from the values obtained from the fits. Essentially, the addition energy can be calculated according to equation 1. Figure 4 shows the calculated (left) and measured (right) results for the polar and azimuthal scans. The usefulness of this verification is primarily for evaluation of issues such as adequacy of the proposed model, signal to noise ratio, and an overall picture of what can be resolved for this two electron system. An important issue mentioned previously was that of ensemble measurements. In this experiment, one obtains a more reliable evaluation of the g-tensor as one is aver-

aging over many different spin configurations which are temperature and magnetic field dependent. This experiment thus provides a more representative description of g-tensor in nanostructures.

In summary, we were able to infer the g-tensor for the s and p shells of self-assembled QDs. We found that for the s-shell the g-tensor was quite anisotropic, reflecting the confinement potential details. For the in-plane component and for the p-shell, the modulus of the inferred g-factors were very close to the bulk GaAs value. Finally, we found that for the p-shell the g-tensor was isotropic within our experimental resolution, which is consistent with wavefunction having a node at the QD center and being more delocalized along the growth direction. We acknowledge the financial support by CNPq, FAPESP and HP Brazil, and the usage of the high magnetic field facility at GPO/IFGW - UNICAMP.

- 
- [1] S. A. Wolf, D. D. Awschalom, R. A. Buhrman, J. M. Daughton, S. von Molnár, M. L. Roukes, A. Y. Chtchelkanova, and D. M. Treger *Science* **294**, 1488 (2001).
  - [2] D. Loss and D.P. DiVincenzo, *Phys. Rev. A* **57**, 120 (1998).
  - [3] L. M. Roth *et al.*, *Phys. Rev.* **114**, 90 (1959).
  - [4] R. J. Elliot, *Phys. Rev.* **96**, 266 (1954).
  - [5] for example, C. Weisbuch and C. Hermann, *Phys. Rev. B* **15**, 816 (1977).
  - [6] *Electron Paramagnetic Resonance of Transition Ions*, A. Abragam, Clarendon Press, Oxford, 1970.
  - [7] L. M. Roth, *Phys. Rev.* **118**, 1534 (1960)
  - [8] C. Calero, E. M. Chudnovsky, and D. A. Garanin, *Phys. Rev. Lett.* **95**, 166603 (2005).
  - [9] A. Malinowski and R. T. Harley, *Phys. Rev. B* **62**, 2051 (2000)
  - [10] M. Oestreich, A. P. Heberle, W. W. Rühle, R. Nötzel and K. Ploog, *Europhys. Lett* **37** (7), 399-404 (1995).
  - [11] J. R. Petta and D. C. Ralph *Phys. Rev. Lett.* **89** 156802 (2002); J. R. Petta and D. C. Ralph *Phys. Rev. Lett.* **87** 266801 (2001).
  - [12] S. Lindemann, T. Ihn, T. Heinzl, W. Zwerger, K. Ensslin, K. Maranowski, and A. C. Gossard, *Phys. Rev. B* **66**, 195314 (2002).
  - [13] R. Hanson *et al.*, *Phys. Rev. Lett.* **91**, 196802 (2003)
  - [14] R. J. Warburton *et al.*, *Phys. Rev. B* **58**, 16221 (1998).
  - [15] Lixin He, Alex Zunger *cond-mat/0511041* v1 (2005).
  - [16] M. Bayer *et al.*, *Phys. Rev. Lett.* **82**, 1748 (1999)
  - [17] A. R. Goñi *et al.*, *Jpn. J. Appl. Phys.* **39**, 3907-3914 (2000).
  - [18] G. Medeiros-Ribeiro *et al.*, *Appl. Phys. Lett.* **80**, 4229 (2002).
  - [19] G. Medeiros-Ribeiro *et al.*, *Appl. Phys. A* **77**, 725 (2003).
  - [20] C. E. Pryor, and M. E. Flatté, *Phys. Rev. Lett.* **96**, 026804 (2006).
  - [21] G. Medeiros-Ribeiro, F. G. Pikus, P. M. Petroff, and A. L. Efros, *Phys. Rev. B* **55**, 1568 (1997).
  - [22] T. Nakaoka *et al.*, *Phys. Rev. B* **71**, 205301 (2005)
  - [23] M. T. Björk *et al.*, *Phys. Rev. B* **72**, 201307(R)(2005)